

Band structure tunability in MoS₂ under interlayer compression: A DFT and GW study

C. Espejo*

*Programa de Nanociencias y Nanotecnología, Centro de Investigación y de Estudios Avanzados del I.P.N. (CINVESTAV),
Libramiento Norponiente 2000, C.P. 76230 Querétaro, Mexico and**Departamento de Ciencias Básicas, Universidad de Bogotá Jorge Tadeo Lozano, Carrera 4 22-61 Bogotá, Distrito Capital, Colombia*

T. Rangel†

*Institute of Condensed Matter and Nanosciences (IMCN), NAPS, Université Catholique de Louvain, Chemin des Étoiles 8,
1348 Louvain-la-Neuve, Belgium*

A. H. Romero

*Physics Department, West Virginia University, P.O. Box 6315, Morgantown, West Virginia 26506, USA,**Max Planck Institute for Microstructure physics, Weinberg 2, 06120, Germany, and**Unidad Queretaro, CINVESTAV, Libramiento Norponiente 2000, CP 76230, Queretaro, Mexico*

X. Gonze and G.-M. Rignanese

*Institute of Condensed Matter and Nanosciences (IMCN), NAPS, Université Catholique de Louvain, Chemin des Étoiles 8,
1348 Louvain-la-Neuve, Belgium and European Theoretical Spectroscopy Facility*

(Received 31 January 2013; published 17 June 2013)

The electronic band structures of MoS₂ monolayer and 2H1 bulk polytype are studied within density-functional theory (DFT) and many-body perturbation theory (GW approximation). Interlayer van der Waals (vdW) interactions, responsible for bulk binding, are calculated with the postprocessing Wannier functions method. From both fat bands and Wannier functions analysis, it is shown that the transition from a direct band gap in the monolayer to an indirect band gap in bilayer or bulk systems is triggered by medium- to short-range electronic interactions between adjacent layers, which arise at the equilibrium interlayer distance determined by the balance between vdW attraction and exchange repulsion. The semiconductor-to-semimetal (S-SM) transition is found from both theoretical methods: around $c = 10.7 \text{ \AA}$ and $c = 9.9 \text{ \AA}$ for DFT and GW, respectively. A metallic transition is also observed for the interlayer distance $c = 9.7 \text{ \AA}$. Dirac conelike band structures and linear bands near Fermi level are found for shorter c lattice parameter values. The VdW correction to total energy was used to estimate the pressure at which S-SM transition takes place from a fitting to a model equation of state.

DOI: [10.1103/PhysRevB.87.245114](https://doi.org/10.1103/PhysRevB.87.245114)

PACS number(s): 71.15.Mb, 71.10.-w, 71.30.+h, 71.20.-b

I. INTRODUCTION

New physical properties exhibited by matter down to the nano scale have raised enormous amounts of experimental and theoretical work. The understanding of the behavior of nanostructured materials and joined advances in synthesis techniques have allowed for the design of systems with desirable properties.

Among the most promising new materials, let us highlight two-dimensional (2D) systems, such as graphene.^{1,2} Their appeal is remarkable, not only for technology, but also for basic science, since new phenomena have been discovered and, in some cases, because 2D materials serve as almost ideal systems where theoretical models can be tested against empirical data.³ Electrons at the K point of the Brillouin zone of graphene behave as massless Dirac fermions, demonstrating a condensed-matter system exhibiting quantum electrodynamical processes.⁴ High electron mobility, vanishing effective mass, and anomalous quantum Hall effect have been observed in graphene, placing it at the top of promising materials for nano technological applications.^{5,6}

Theoretical studies and experimental evidence on the remarkable properties of graphene have produced a renewed interest in 2D crystals. An important source of these systems are the transition-metal dichalcogenides (TMDs),⁷ and MoS₂ is perhaps one the most distinguished representatives of this

family. Contrary to graphene, the finite band gap of MoS₂ monolayer readily makes it suitable for electronic applications such as the recently reported monolayer MoS₂ transistor.⁸

It is well known that MoS₂ undergoes a band-gap transition going from direct gap in the isolated monolayer⁹⁻¹² to indirect band gap in the case of bilayer or for bulk systems.¹³⁻¹⁵ In previous works,^{14,16} the band gap dependence upon both the number of layers and the interlayer distance was determined. On opposite sides of the scale we have the isolated monolayer and the equilibrium bulk. The evolution of the band gap was mapped as a function of the number of layers, placing them at the experimental bulk interlayer distance. The result is that the gap goes from direct to indirect while decreasing its magnitude from 1.8 to 0.86 eV.¹⁶ The latter values are not in total agreement with the experimental data^{15,16} given the theoretical constrains which prevent DFT to predict band gaps accurately. However, the global behavior is well described. Experimental realization of phototransistors which exploit the dependence of the gap with the number of layers has been reported.^{17,18}

Very recently, there have been theoretical reports demonstrating that MoS₂ monolayers^{19,20} and bilayers undergo a semiconductor-to-semimetal (S-SM) transition under biaxial strain²¹ and also compressive uniaxial strain in TMD bilayer systems.²² A similar behavior has also been predicted if an

electric field is applied perpendicular to the layers.²³ These studies are examples of the great band structure tunability found on MoS₂ few-layer systems.

Here we show that bulk also exhibit such S-SM transition in the case of short interlayer distance, due to uniaxial strain perpendicular to the layers. We explore this additional degree of freedom, which could be useful for band engineering purposes, from van der Waals-corrected DFT and MBPT calculations. The inclusion of van der Waals interactions is important in order to obtain an accurate description of the energetics involved in the uniaxial compression of the layers.²⁴ We found the appearance of an asymmetrical Dirac conelike structure at the *K* point below the Fermi level at the semimetal phase which is preserved for shorter interlayer distances leading to a metallic transition.

The paper is organized as follows. The theoretical methods and several calculation parameters are presented in the first section. Results and discussions are found next, devoting the first part to the structural characterization by using van der Waals-corrected DFT. Then the study of electronic structure as a function of *c* lattice parameter follows for two cases, one where the layer geometry is kept fixed at the monolayer values and a second one in which for each *c* value we perform in-plane relaxation of layers. MBPT results for the bulk are presented next and concluding remarks are given in the last section.

II. THEORETICAL METHODS

A. vdW-corrected DFT and band structure

Van der Waals (vdW) interactions are crucial in the determination of the equilibrium configurations in layered materials such as MoS₂. These interactions are out of range for common used exchange-correlation (XC) functionals.²⁵ Therefore, we have used our recent implementation in ABINIT²⁶ of a method which makes it possible to calculate vdW energies from maximally localized Wannier functions (MLWFs) of the system,^{27,28} also known as the vdW-WF method. This method is based in the Anderson, Langreth and Lundqvist (ALL) functional²⁹ which treats the long-range correlation energy, responsible for vdW interactions, as a postprocessing correction to the ground-state energy. VdW energy is calculated from a double spatial integral of the ground-state electronic density. In the vdW-WF method, the actual electronic density is replaced with those ones coming from the Wannier functions of the system which are, in turn, approximated by hydrogenlike functions, characterized by its spreads and centers. The latter approximations allow for an important reduction of the computational power needed to evaluate the double spatial integral of the ALL functional, resulting in an additional time comparable to a single step of the self-consistent field computation. In general, the spreads of MLWFs change only by a small amount when the ions are displaced by short distances. Therefore, for infinitesimal displacements of the interacting fragments the spread change is negligible and they can be assumed to be constant, giving raise to a computation method to evaluate the vdW forces analytically, as it was clearly introduced in Ref. 28. Since the localization of Wannier functions is performed through the interface to the WANNIER90 (Ref. 30) program, the inclusion of these forces into a geometry

optimization procedure is cumbersome and is not yet available in ABINIT. Exchange and correlation energies are recommended to be treated with revPBE functional,³¹ avoiding spurious binding coming from exchange.²⁷ However, we found that the vdW-WF correction to the results obtained with the PBE functional³² leads to equilibrium parameters which are in better agreement with experimental data for MoS₂ than those obtained from the vdW-WF correction to revPBE calculations. VdW interactions calculation demands convergence of total energy as small as a few meV; therefore, a cutoff energy of 50 Ha and a $8 \times 8 \times 2$ Brillouin zone sampling were used throughout. Molybdenum semicore states *4s* and *4p* were included for both structural and band-structure calculations. The corresponding atomic pseudopotentials were generated with the code APE.³³ Starting from geometrical parameters found in the literature for MoS₂ monolayer,¹⁴ we performed structural relaxation until the maximum force on each atom was less than 10^{-5} Ha/bohr. Once the monolayer structure was determined, we optimized the unit cell geometry of the solid by computing the interlayer binding energy as a function of *c* lattice parameter while keeping the layer geometry fixed at their isolated configuration. In a second case, we perform in-plane relaxation for each value of *c* until stress tensor components were less than 0.001 Gpa, as opposed to previous calculations for bilayer systems where the layer geometry was kept fixed.²² The number of units cells along each lateral primitive vector was 20 and 3 unit cells normal to the layers in both cases, for which convergence of vdW corrections was reached.

B. MBPT band structure

MBPT is well established as an accurate method to predict band gaps in solids, based on the one-electron Green's function *G* and the screened Coulomb potential *W*. In this paper, we adopt the standard so-called *G*₀*W*₀ technique proposed in Ref. 34. The Kohn-Sham (KS) eigenvalues E^{KS} are taken as a zeroth-order perturbation to the quasiparticle (QP) eigenenergies E^{QP} as

$$E_i^{QP} = E_i^{KS} + \langle \psi_i^{KS} | \Sigma - V_{xc} | \psi_i^{KS} \rangle, \quad (1)$$

where V_{xc} is the XC potential and the self-energy Σ is a non-Hermitian, frequency-dependent, and nonlocal operator. The non-Hermitian part of the self-energy, which gives rise to QP lifetimes, is neglected. The KS wave functions (ψ^{KS}) are considered to be close to the QP ones; hence, they are not modified. Recent results of quasiparticle self-consistent *GW* (QSGW) approach on bulk, monolayer, and bilayer MoS₂ have shown better agreement with absorption experiments³⁵ than *G*₀*W*₀ at a larger computational cost, though. The plasmon pole model (PPM) of Ref. 36 was used to simplify the frequency dependency of Σ . Recently, it has been shown that the plasmon-pole approximation is suitable for systems with *d* electrons,^{37,38} as is the case with MoS₂. This PPM achieves the best agreement with more robust integration methods.³⁹ In this work the relaxed DFT bulk structures (including vdW forces) were used. We found it crucial to include Mo semicore states *4s* and *4p* to obtain physical QP energies. For the *G*₀*W*₀ calculations, DFT-LDA fhi98PP⁴⁰ pseudopotentials were used since *G*₀*W*₀ on top of LDA has proven successful in predicting band gaps in weakly correlated materials.⁴¹

In the G_0W_0 sums 300 bands were included. An energy cutoff of 7.0 and 30 hartrees were used to generate the polarizability and the exchange part of Σ , respectively. This choice of parameters achieves a convergence in the QP eigenvalues of 0.01 eV. Furthermore, the QP energies were computed for the same k mesh used in the ground-state calculations. The MBPT band structures presented here were interpolated using MLWFs, as explained elsewhere.⁴²

III. RESULTS AND DISCUSSION

First, we present our results for the structural optimization and electronic structure calculations from vdW-corrected DFT and DFT-GGA methods respectively, as applied for the MoS₂ monolayer and 2H1 bulk polytype. Then, the G_0W_0 method is applied for the study of the S-SM transition predicted from DFT.

A. Structural characterization from DFT + vdW – WF

MoS₂ is a layered material composed of weakly bonded sheets of trigonal prismatic symmetry. Figure 1 shows the unit cell with six atoms and the Wannier centers used to evaluate the vdW correction to the energy. In Table I, the structural parameters obtained for the monolayer and bulk for several values of c lattice parameters are displayed. Calculated in-plane lattice parameters for the isolated monolayer are found to be in good agreement with the corresponding experimental bulk values, with a difference of only 0.53%. With small variations, this result is also obtained with several XC functionals and from all-electron calculations¹¹ as well. Therefore, it is customary that in previous studies on the electronic structure of MoS₂ monolayers, bulk, and or few-layer systems, the internal geometry of the layers was set equal to either the reported experimental bulk values¹⁴ or to relaxed monolayer parameters.¹⁵ However, as has been reported, the electronic structure is highly sensitive to both the internal structural parameters of the layers and the interlayer distance, which may undergo large changes in the case of applied strain^{19–21} or applied electric fields.²³ In the case of uniaxial strain studied in this work, such large changes in geometry are also important and determine the S-SM transition, as explained below. In general, as long as the length of the c parameter is reduced, an increment of the cell parameters a and b is

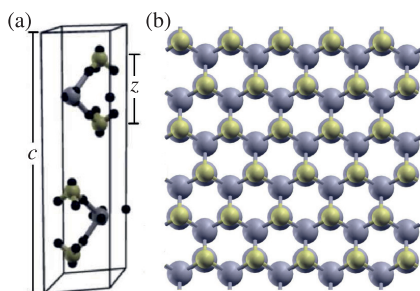


FIG. 1. (Color online) (a) 2H1 MoS₂ unit cell. S atoms (yellow) in one layer are right on top of Mo atoms (gray) of the second layer. The Wannier centers are represented as small black spheres. z is the vertical distance between S atoms (considered as the layer width). (b) Top view of the MoS₂ crystal.

TABLE I. Calculated MoS₂ monolayer and bulk structural parameters and experimental values from Ref. 13. Evolution of in-plane effective mass for holes and electrons is given in the two last columns.

	a (Å)	c (Å)	z (Å)	m_h^*/m_e	m_e^*/m_e
1L	3.178		3.138	-1.490	1.280
Bulk	3.253	10.7	2.999	-0.469	1.024
	3.248	10.8	3.011	-0.507	1.042
	3.241	10.9	3.023	-0.677	1.071
	3.236	11.0	3.034	-0.716	1.141
	3.199	12.5	3.115	-1.744	1.601
Exp.	3.160	12.294	3.172		

observed. On the other hand, the layer width z depends linearly with c , except for $c > 11.2$ Å, the starting point of saturation towards the isolated monolayer value $z = 3.138$ Å.

The energetics of interlayer bonding has two main ingredients, namely, the attractive vdW interactions and the exchange repulsion between layers. Figure 2 displays the interaction energy per layer and per unit surface area from both PBE and the vdW-corrected functional. Each curve has been calculated twice, either fixing the layer geometry to that of the isolated monolayer or allowing the layers to relax for each c value. The reference energy was defined as the total energy of the unit cell for $c = 30$ Å upon in-plane relaxation. In both cases the PBE curve has no minimum, indicating that from this level of theory the system would be unstable. On the other hand, once we add the correlation energy calculated from the vdW-WF method (red triangles in Fig. 2), the obtained curves show a minimum at $c \sim 12.5$ Å. Theoretical results⁴³ from random phase approximation, vdW-DF, and PBE-D methods are displayed for comparison. DFT + vdW-WF provides both interlayer distance and interplanar binding energy which are in close agreement to other approaches for vdW interactions in DFT. From the results, it is clear that the energy cost of layer relaxation, the so-called stabilization energy, is an important component of the total energy which must be considered. In Fig. 2 the stabilization energy is the energy difference between

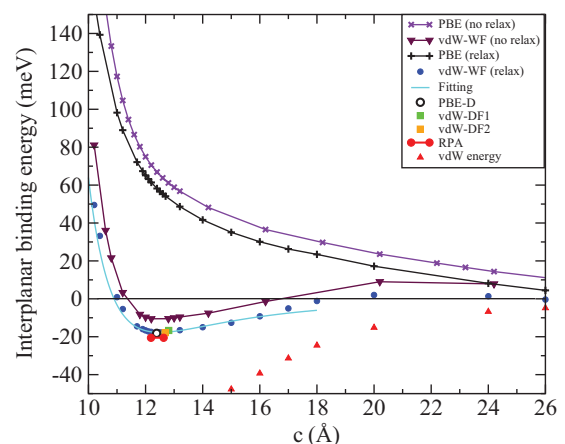


FIG. 2. (Color online) Interaction energy per layer and primitive surface unit. Comparison with results from several DFT methods. Present calculations: PBE (no relaxation), PBE (relaxed), vdW correction energy and vdW-WF (also fit to the latter values). Other results from Ref. 43.

the PBE (non-relaxed) and PBE (relaxed) curves for $c = 30 \text{ \AA}$. Because of this energy, the vdW-WF-corrected interplanar binding energy, for the fixed-layers case, becomes positive at $c \sim 17 \text{ \AA}$. It is worth noticing that the vdW-corrected, relaxed-layers energy curve displays a small bump over the zero energy. This unphysical result could be attributed to a small noncompensated repulsion between the layers coming from the long-range behavior of the PBE functional. From a fitting to a quadratic function around the minimum we obtain a bulk modulus of 29.11 GPa, which compares with 39 GPa obtained from vdW-DF⁴⁴ using a fixed-layers approach. Layer relaxation produces a softening of both elastic constants and bulk modulus with respect to the fixed-layers case.⁴³ Cubic splines are used to compute the derivative of unit cell total energy with respect to the volume V when assessing the pressure at which electronic transitions may occur ($P = -\partial U/\partial V$).

B. Direct to indirect band-gap transition revisited

Several theoretical works have shown that the direct band gap of MoS₂ monolayer is replaced with an indirect band gap in systems with more than one layer.^{11,15} This effect is proportional to both the number of layers considered and its proximity.¹⁴ Experimental evidence which confirms theoretical descriptions has also been obtained.^{9,13} A direct band gap is then characteristic of isolated monolayers only. The presence of neighbor layers changes it for an indirect gap even with just one additional layer.

Hence, two limiting cases are the MoS₂ isolated monolayer and the bulk system. Calculated projected densities of states (PDOS) for these systems are displayed in Fig. 3. Even though the changes of PDOS are small when going from the isolated monolayer to the bulk case, band structure displays the gap transition. It is found that the main contribution to

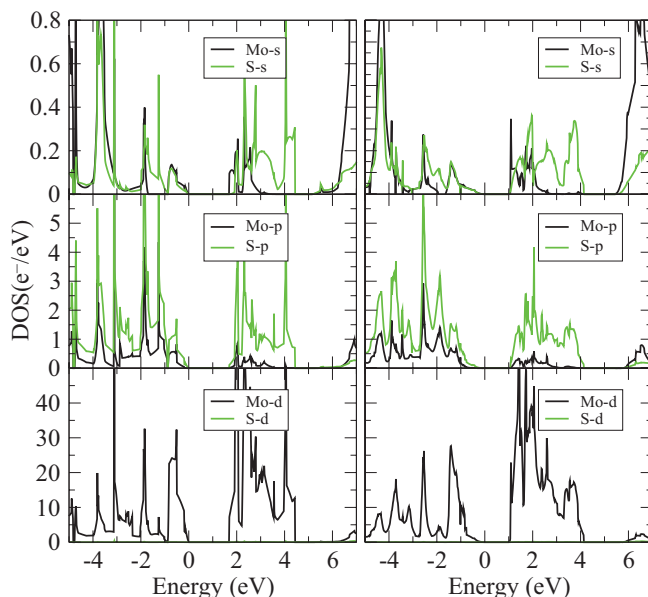


FIG. 3. (Color online) Projected densities of states for (left) monolayer and (right) bulk at equilibrium. Contributions of atomic states of sulfur and molybdenum are in green and black, respectively.

valence-band maximum (VBM) and conduction-band minimum (CBM) of monolayer comes from Mo d states, as well as for the bulk case, followed by the p states contribution. On the other hand, the contribution from sulfur states undergoes a very small change for the two systems.

Although it has been claimed that this effect is due to vdW interactions,⁴⁵ we are calculating it from a non-self-consistent method which neither affect nor modifies the electronic density as it is originally obtained from the self-consistent GGA calculation. Therefore, the change in the band gap would be the result of electronic interactions different from vdW although the proximity of layers is indeed caused by them.

C. Evolution of band structure as a function of c lattice parameter

S-SM transition in MoS₂ monolayer and bilayer systems due to biaxial strain has been reported previously.^{19–21} In these studies both tensile and compressive strains are applied homogeneously along each lattice vector parallel to the layers. S-SM transition is reported around 10% and 15% for tensile and compressive strain, respectively, in the monolayer.

In the case of bulk MoS₂ there is an additional degree of freedom for a similar transition, corresponding to the application of uniaxial compressive strain normal to the layers. As a consequence, the gradual reduction of interlayer distance fosters confinement of charge at the Mo planes while reducing layer width. A similar behavior has been reported in the case of applied electric fields normal to the layers.²³

The resulting modification of electronic band structure is characterized by a progressive reduction of the indirect band gap magnitude between the Γ point at the valence band and a midpoint between K and Γ in the conduction band. Figure 4 shows the evolution of the band gap as a function of the c lattice parameter. From these data it is estimated that the S-SM transition will occur at $c = 10.7 \text{ \AA}$, equivalent to a compressive strain of about 14.4% (see Figs. 4 and 5). From the cubic spline performed on the values of corrected interaction energy as a

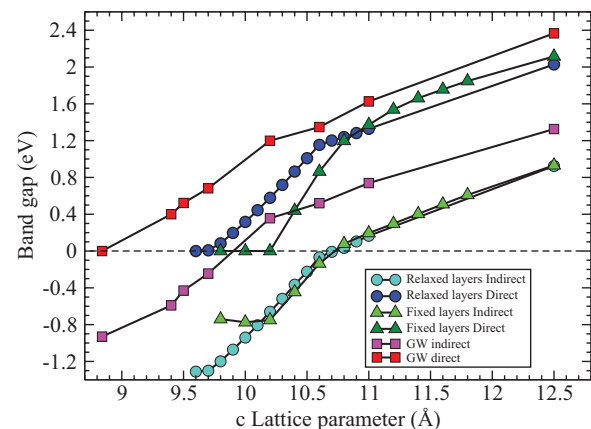


FIG. 4. (Color online) Evolution of both direct and indirect band gaps of 2H1 MoS₂ with the c lattice parameter. Circles, DFT, relaxed layers; triangles, DFT, fixed layers; squares, G_0W_0 on DFT relaxed layers. Negative gap values indicate that the conduction band bottom is below the valence band top, showing the S-SM transition. The metallic transition occurs when the direct gap goes to zero.

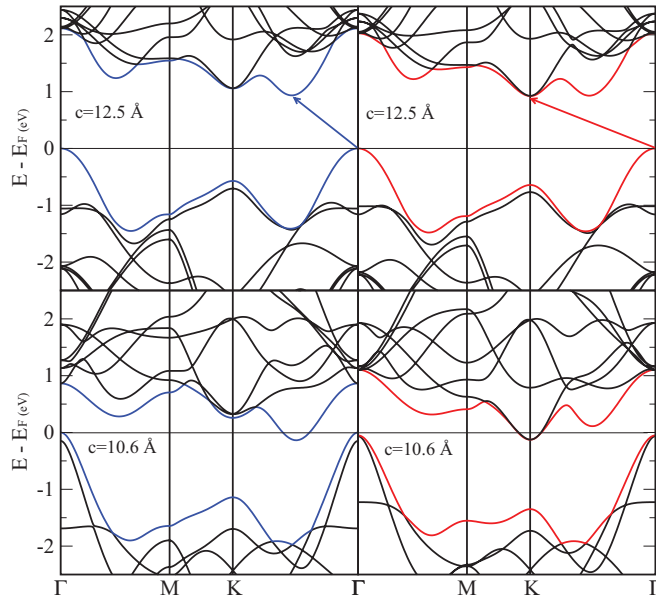


FIG. 5. (Color online) Semiconductor-to-semimetal transition. (Left) Fixed-layers case, last valence band and first conduction band in blue. (Right) Relaxing-layer case, last valence band and first conduction band in red.

function of unit cell volume, our estimated pressure at which this electronic transition may occur is 29.11 GPa.

In case of further compression, the direct band gap on Γ is reduced until a metallic state of null gap is reached. In Fig. 4, a positive change in the slope for both the direct and the indirect gap is observed once the system has come to the semimetallic state. This trend is more marked for the case in which layers are free to relax than if its geometry is fixed. While the slopes for both gaps are the same in the case of relaxing layers, for the rigid-layers case the direct gap has a larger slope as compared to that of the indirect gap. Therefore, in the latter case, the metallic transition is reached for a larger c if compared to relaxing layers. An additional interesting feature of the electronic structure evolution is the reduction of the in-plane effective masses and the appearance of straight bands near Γ and K at the Fermi level. For small-enough c , Dirac conelike structures appear at three points of the first Brillouin zone in the rigid-layers case while a similar band structure is found at Γ for relaxing layers. It should be noticed that in the latter case a single-band Dirac cone is found at K , with its vertex approximately at 1.3 meV below the Fermi level; see dashed circle of Fig. 6. This linear band is almost degenerated with a normal parabolic band. At the G_0W_0 level the latter structure gives rise to a full Dirac cone for $c = 8.84 \text{ \AA}$.

Even though we have simulated a bulk system, short interlayer distance fosters the confinement of charge at monolayer planes, an expected effect on truly 2D crystals. This is only possible due to the weak chemical interactions between adjacent layers preventing the formation of bonds. As was discussed before, there is a dependence of layer width on c , in a similar fashion as for the case of biaxial strain.¹⁹⁻²¹ This reduction is associated with a greater charge confinement along the Mo planes which, in turn, provokes electronic transitions and eventually the appearance of conical bands.

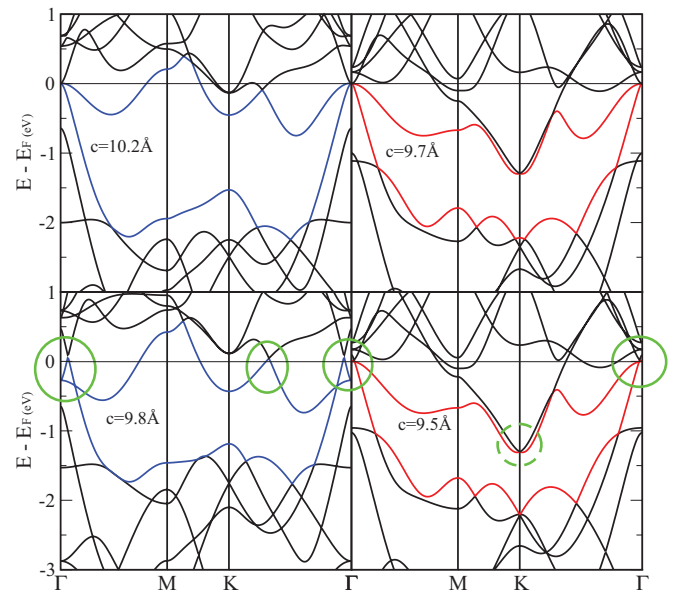


FIG. 6. (Color online) Metallic transition. (Left) Fixed-layers geometry. (Right) Relaxed layers. Valence bands are closer to conduction bands in the case of fixed-layers than in the relaxing-layers case. There is a difference of 0.5 \AA in the transition-lattice parameter between both cases. Regions where Dirac conelike bands appear are enclosed by green circles.

D. G_0W_0 band structure

In Figs. 7 and 8, results from G_0W_0 calculations are displayed. The geometries obtained for structural relaxations at the DFT level for each c value were used. One of the main characteristics of the G_0W_0 -corrected band structures is a general increment of gap values. The latter has as a

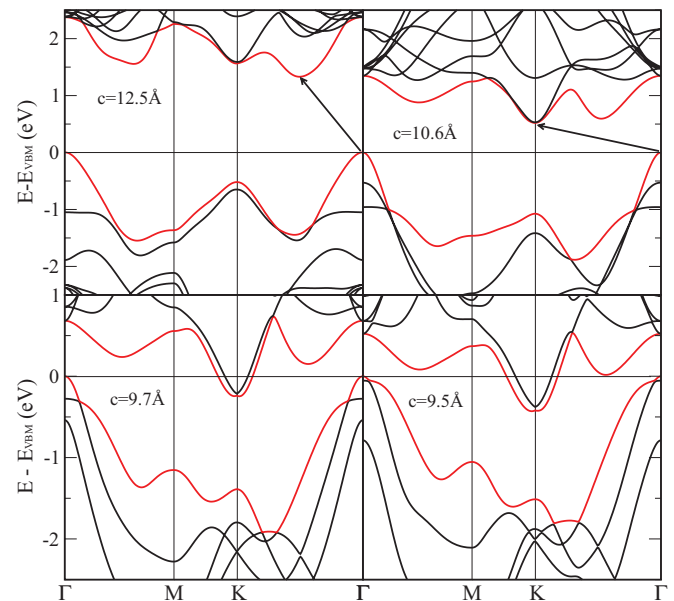


FIG. 7. (Color online) G_0W_0 band structures for several values of c lattice parameter. For each c value the obtained geometries at the DFT level upon in-plane relaxation were used. Energies referred to the VBM.

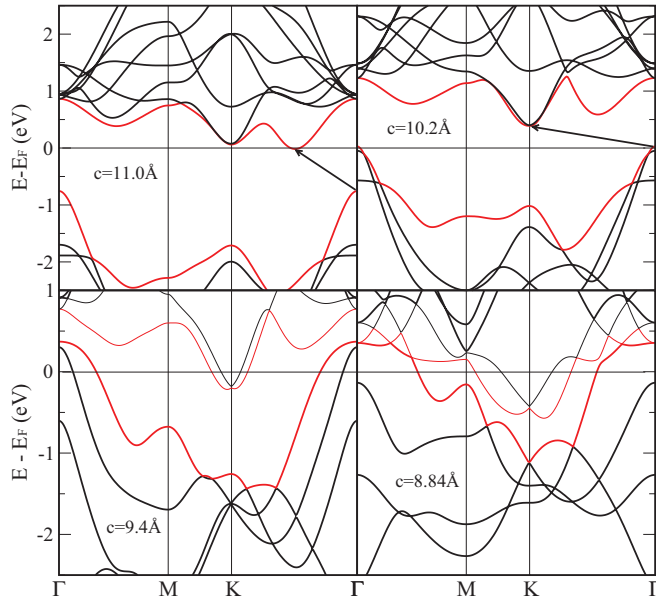


FIG. 8. (Color online) G_0W_0 band structures for several values of the c lattice parameter. For each c value the obtained geometries at the DFT level upon in-plane relaxation were used. Energies referred to the Fermi level.

consequence that both the S-SM transition as well as the SM-M transition occur for shorter interlayer spacing, as can be seen in Fig. 4. Comparison with DFT results shows that the conical structures remain only at the K point of the Brillouin zone. However, a set of linear bands and a discontinuity in the second derivative of the dispersion relation appears in the same symmetry point just after the semimetal transition, while for the DFT case, these characteristics arise once the system reaches the metallic state. From MBPT calculation, the cone is placed at 0.5 eV below Fermi energy, while from DFT it is placed at K , 1.65 eV below the Fermi energy. Apart from being located below the Fermi level, the main difference with graphene Dirac cones is that linear bands do not have the same extension in reciprocal space around the K point for electrons and holes, as can be seen in Figs. 8 and 10 for $c = 8.84 \text{ \AA}$.

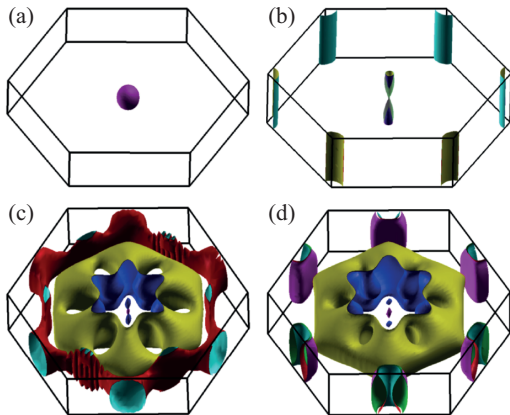


FIG. 9. (Color online) Fermi surfaces for (a) bulk in equilibrium, $c = 12.5 \text{ \AA}$; (b) semimetal state, $c = 10.6 \text{ \AA}$; (c) metallic transition $c = 9.7 \text{ \AA}$; and (d) appearance of conical bands, $c = 9.4 \text{ \AA}$.

Finally, in Fig. 9, we present the evolution of the Fermi surface, calculated at the DFT level for relaxed layers. The Fermi surface increases its complexity when going from the normal semiconductor state up to the metallic transition. For semimetallic and metallic states, Fermi surface share a similar structure with TlBiTe, which is also a semimetal with one Dirac cone [in that case located on Γ (Ref. 46)]. For energies around the Dirac point, there are closed Fermi surfaces with C_6 symmetry, as observed in Fig. 9(d). Another reported material exhibiting a single Dirac cone on Γ is the topological insulator Bi_2Se_3 (Ref. 47), which is a material composed of quintuple layers weakly bonded by vdW interactions. Clearly, from our calculations, MoS_2 exhibits a behavior resembling topological insulators, induced by great proximity between layers. Band structures showed so far represent the dispersion relation along BZ special lines; hence, a 3D representation of $E(k_x, k_y)$ is desirable. A close-up view of the Dirac pointlike in MoS_2 for $c = 8.84 \text{ \AA}$ is displayed in Fig. 10.

From Fig. 10 it is evident that linear bands, forming conical shapes resembling Dirac cones of graphene, are not only occurring along the special lines passing by K . For the case displayed and for the whole set of performed calculations on relaxed layers, conical bands appear below

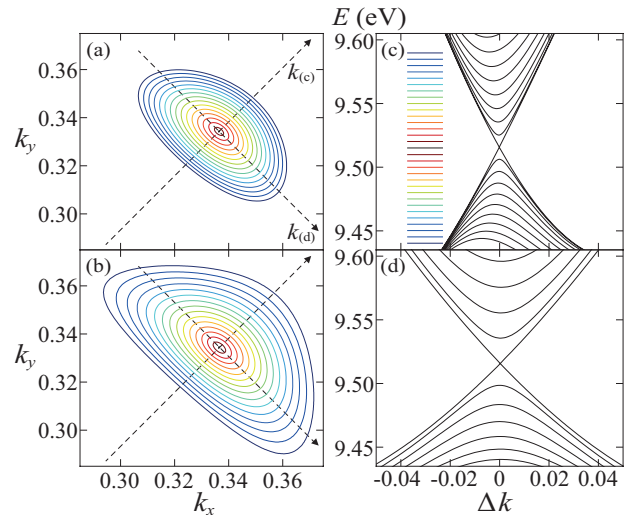


FIG. 10. (Color online) Illustration of the Dirac cone obtained from G_0W_0 calculations for $c = 8.84 \text{ \AA}$ around K . Contour plot of the upper (a) and lower (b) parts of the cone: The isocurves are separated by 0.005 eV. The tip of the cone (in black) is at $k_x = 0.334$ and $k_y = 0.347$ with $E \sim 9.515 \text{ eV}$. The color scheme for the contours of is reported in panel (c). In the upper part of the cone (a), the lowest energies are in red (black); when increasing they turn to yellow (very light gray), green (light gray), cyan (gray), and finally blue (black) for the highest values. In the lower part of the cone (b), it is just the reverse. Cuts through the cone are also reported in panels (c) and (d), following, respectively, the directions $k_{(c)}$ and $k_{(d)}$ as indicated in panel (a). The cuts which show an intersection are obtained by taking the axes which pass through the tip. In panel (c), the other curves are obtained by translating the $k_{(c)}$ axis along the $k_{(d)}$ axis by steps of 0.005. The cuts provide the energy (in eV) as a function of the distance Δk with respect to the tip along $k_{(c)}$. In panel (c), it is just the reverse. The warping effect is clearly demonstrated by the difference in the slopes of the cones in panels (c) and (d).

E_F . This prevents the linear bands and the Dirac-like point from governing the overall electronic behavior of the system. The experimental identification of Dirac cones away from the Fermi level is nevertheless possible, as done in Ref. 48. The only case with conical bands at E_F was obtained at the DFT level for $c = 9.8$ Å using the monolayer geometry; see Fig. 6. Although this hypothetical system could exhibit some properties associated with relativistic electrons, its physical realization is not feasible.

IV. CONCLUSIONS

We have computed the geometric and electronic properties of bulk MoS₂ under pressure, using different methodologies. The vdW-WF method describes the bonding between MoS₂ layers with an accuracy similar to other postprocessing approaches like DFT-D. Its results compare well with that from self-consistent vdW-DF, although the bulk modulus is underestimated by ~ 10 GPa. MoS₂ band structure tunability under uniaxial pressure was demonstrated from DFT and MBPT approaches. The evolution of both indirect and direct band gaps was calculated as a function of the c lattice parameter. This procedure was realized for two cases: keeping fixed the layers geometry in its isolated configuration and

relaxing the layers at each c value. Semiconductor-to-semimetal transitions were found at $c = 10.7$ Å for both cases at the DFT level, corresponding to a pressure of ~ 30 GPa, while G_0W_0 calculations predict the S-SM transition to occur at $c \sim 9.9$ Å. Appearance of conical bands was demonstrated from both theoretical approaches and for the relaxing and fixed-layers cases. If the relaxed layers geometry is used, the Dirac point is always placed below the Fermi energy.

ACKNOWLEDGMENTS

We would like to acknowledge technical support from Y. Pouillon, A. Jacques, and J.-M. Beuken. This work was supported by the FRS-FNRS through FRFC Projects No. 2.4.589.09.F and No. 2.4645.08, the Communauté française de Belgique, through the Action de Recherche Concertée 07/12-003 “Nanosystèmes hybrides métal-organiques,” the Région Wallonne through WALL-ETSF Project No. 816849. A.H.R. recognizes the support of CONACYT Mexico under Project No. 152153, MICINN of Spain under Grant No. MAT2010-21270-C04-01/03, as well as the Marie-Curie Intra-European Fellowship. C.E. acknowledges financial support from CONACYT Mexico and Universidad de Bogotá Jorge Tadeo Lozano.

*cespejo@qro.cinvestav.mx

[†]Present address: CEA/DAM/DIF, Arpajon, France.

- ¹A. K. Geim and K. S. Novoselov, *Nat. Mater.* **6**, 183 (2007).
- ²R. Mas-Balleste, C. Gomez-Navarro, J. Gomez-Herrero, and F. Zamora, *Nanoscale* **3**, 20 (2011).
- ³A. Grüneis, C. Attaccalite, A. Rubio, D. V. Vyalikh, S. L. Molodtsov, J. Fink, R. Follath, W. Eberhardt, B. Büchner, and T. Pichler, *Phys. Rev. B* **80**, 075431 (2009).
- ⁴K. S. Novoselov, A. K. Geim, S. V. Morozov, D. Jiang, M. I. Katsnelson, I. V. Grigorieva, S. V. Dubonos, and A. A. Firsov, *Nature (London)* **438**, 197 (2005).
- ⁵A. H. Castro Neto, F. Guinea, N. M. R. Peres, K. S. Novoselov, and A. K. Geim, *Rev. Mod. Phys.* **81**, 109 (2009).
- ⁶P. Avouris and C. Dimitrakopoulos, *Mater. Today* **15**, 86 (2012).
- ⁷J. N. Coleman *et al.*, *Science* **331**, 568 (2011).
- ⁸B. Radisavljevic, A. Radenovic, J. Brivio, V. Giacometti, and A. Kis, *Nat. Nano.* **6**, 147 (2011).
- ⁹K. F. Mak, C. Lee, J. Hone, J. Shan, and T. F. Heinz, *Phys. Rev. Lett.* **105**, 136805 (2010).
- ¹⁰Y. Ding, Y. Wang, J. Ni, L. Shi, S. Shi, and W. Tang, *Physica B* **406**, 2254 (2011).
- ¹¹E. S. Kadantsev and P. Hawrylak, *Solid State Commun.* **152**, 909 (2012).
- ¹²S. Lebègue and O. Eriksson, *Phys. Rev. B* **79**, 115409 (2009).
- ¹³T. Böker, R. Severin, A. Müller, C. Janowitz, R. Manzke, D. Voß, P. Krüger, A. Mazur, and J. Pollmann, *Phys. Rev. B* **64**, 235305 (2001).
- ¹⁴T. Li and G. Galli, *J. Phys. Chem. C* **111**, 16192 (2007).
- ¹⁵J. K. Ellis, M. J. Lucero, and G. E. Scuseria, *Appl. Phys. Lett.* **99**, 261908 (2011).

- ¹⁶A. Splendiani, L. Sun, Y. Zhang, T. Li, J. Kim, C.-Y. Chim, and G. Galli, and F. Wang, *Nano Lett.* **10**, 1271 (2010).
- ¹⁷Z. Yin, H. Li, H. Li, L. Jiang, Y. Shi, Y. Sun, G. Lu, Q. Zhang, X. Chen, and H. Zhang, *ACS Nano*, **6**, 74 (2011).
- ¹⁸H. S. Lee, S.-W. Min, Y.-G. Chang, M. K. Park, T. Nam, H. Kim, J. H. Kim, S. Ryu, and S. Im, *Nano Lett.* **12**, 3695 (2012).
- ¹⁹W. S. Yun, S. W. Han, S. C. Hong, I. G. Kim, and J. D. Lee, *Phys. Rev. B* **85**, 033305 (2012).
- ²⁰H. Peelaers and C. G. Van de Walle, *Phys. Rev. B* **86**, 241401 (2012).
- ²¹E. Scalise, M. Houssa, G. Pourtois, V. Afanasev, and A. Stesmans, *Nano Res.* **5**, 43 (2012).
- ²²S. Bhattacharyya and A. K. Singh, *Phys. Rev. B* **86**, 075454 (2012).
- ²³A. Ramasubramaniam, D. Naveh, and E. Towe, *Phys. Rev. B* **84**, 205325 (2011).
- ²⁴T. Bučko, J. Hafner, S. Lebègue, and J. G. Ángyán, *J. Phys. Chem. A* **114**, 11814 (2010).
- ²⁵J. Klimes and A. Michaelides, *J. Chem. Phys.* **137**, 120901 (2012).
- ²⁶C. Espejo, T. Rangel, Y. Pouillon, A. H. Romero, and X. Gonze, *Comput. Phys. Commun.* **183**, 480 (2012).
- ²⁷P. L. Silvestrelli, *Phys. Rev. Lett.* **100**, 053002 (2008).
- ²⁸P. L. Silvestrelli, *J. Phys. Chem. A*, **113**, 5224 (2009).
- ²⁹Y. Andersson, D. C. Langreth, and B. I. Lundqvist, *Phys. Rev. Lett.* **76**, 102 (1996).
- ³⁰A. A. Mostofi, J. R. Yates, Y.-S. Lee, I. Souza, D. Vanderbilt, and N. Marzari, *Comput. Phys. Commun.* **178**, 685 (2008).
- ³¹Y. Zhang and W. Yang, *Phys. Rev. Lett.* **80**, 890 (1998).
- ³²J. P. Perdew, K. Burke, and M. Ernzerhof, *Phys. Rev. Lett.* **77**, 3865 (1996).
- ³³M. J. Oliveira and F. Nogueira, *Comput. Phys. Commun.* **178**, 524 (2008).

- ³⁴S. V. Faleev, M. van Schilfgaarde, and T. Kotani, *Phys. Rev. Lett.* **93**, 126406 (2004).
- ³⁵T. Cheiwchanchamnangij and W. R. L. Lambrecht, *Phys. Rev. B* **85**, 205302 (2012).
- ³⁶R. W. Godby and R. J. Needs, *Phys. Rev. Lett.* **62**, 1169 (1989).
- ³⁷M. Stankovski, G. Antonius, D. Waroquiers, A. Miglio, H. Dixit, K. Sankaran, M. Giantomassi, X. Gonze, M. Côté, and G.-M. Rignanese, *Phys. Rev. B* **84**, 241201 (2011).
- ³⁸A. Miglio, D. Waroquiers, G. Antonius, M. Giantomassi, M. Stankovski, M. Côté, X. Gonze, and G.-M. Rignanese, *Eur. Phys. J. B* **85**, 1 (2012).
- ³⁹R. Shaltaf, G.-M. Rignanese, X. Gonze, F. Giustino, and A. Pasquarello, *Phys. Rev. Lett.* **100**, 186401 (2008).
- ⁴⁰M. Fuchs and M. Scheffler, *Comput. Phys. Commun.* **119**, 67 (1999).
- ⁴¹M. van Schilfgaarde, T. Kotani, and S. Faleev, *Phys. Rev. Lett.* **96**, 226402 (2006).
- ⁴²D. R. Hamann and D. Vanderbilt, *Phys. Rev. B* **79**, 045109 (2009).
- ⁴³T. Björkman, A. Gulans, A. V. Krasheninnikov, and R. M. Nieminen, *Phys. Rev. Lett.* **108**, 235502 (2012).
- ⁴⁴D. C. Langreth, M. Dion, H. Rydberg, E. Schröder, P. Hyldgaard, and B. I. Lundqvist, *Int. J. Quantum Chem.* **101**, 599 (2005).
- ⁴⁵S. W. Han, H. Kwon, S. K. Kim, S. Ryu, W. S. Yun, D. H. Kim, J. H. Hwang, J.-S. Kang, J. Baik, H. J. Shin, and S. C. Hong, *Phys. Rev. B* **84**, 045409 (2011).
- ⁴⁶Y. L. Chen, Z. K. Liu, J. G. Analytis, J.-H. Chu, H. J. Zhang, B. H. Yan, S.-K. Mo, R. G. Moore, D. H. Lu, I. R. Fisher, S. C. Zhang, Z. Hussain, and Z.-X. Shen, *Phys. Rev. Lett.* **105**, 266401 (2010).
- ⁴⁷H. Zhang, C.-X. Liu, X.-L. Qi, X. Dai, Z. Fang, and S.-C. Zhang, *Nat. Phys.* **5**, 438 (2009).
- ⁴⁸M. Yankowitz, J. Xue, D. Cormode, J. D. Sanchez-Yamagishi, K. Watanabe, T. Taniguchi, P. Jarillo-Herrero, P. Jacquod, and B. J. LeRoy, *Nat. Phys.* **8**, 382 (2012).